

Ultrathin Ga₂O₃ Glass: A Large-Scale Passivation and Protection Material for Monolayer WS₂

Matthias Wurdack,^{*} Tinghe Yun, Eliezer Estrecho, Nitu Syed, Semonti Bhattacharyya, Maciej Pieczarka, Ali Zavabeti, Shao-Yu Chen, Benedikt Haas, Johannes Müller, Mark N. Lockrey, Qiaoliang Bao, Christian Schneider, Yuerui Lu, Michael S. Fuhrer, Andrew G. Truscott, Torben Daeneke,^{*} and Elena A. Ostrovskaya^{*}

Atomically thin transition metal dichalcogenide crystals (TMDCs) have extraordinary optical properties that make them attractive for future optoelectronic applications. Integration of TMDCs into practical all-dielectric heterostructures hinges on the ability to passivate and protect them against necessary fabrication steps on large scales. Despite its limited scalability, encapsulation of TMDCs in hexagonal boron nitride (hBN) currently has no viable alternative for achieving high performance of the final device. Here, it is shown that the novel, ultrathin Ga₂O₃ glass is an ideal centimeter-scale coating material that enhances optical performance of the monolayers and protects them against further material deposition. In particular, Ga₂O₃ capping of monolayer WS₂ outperforms commercial-grade hBN in both scalability and optical performance at room temperature. These properties make Ga₂O₃ highly suitable for large-scale passivation and protection of monolayer TMDCs in functional heterostructures.

2D atomically thin monolayers of transition metal dichalcogenide crystals (TMDCs) are highly optically active, direct bandgap semiconductors that have emerged as a promising platform for future low-energy electronics, optoelectronics, and photonics.^[1–4] Extensive research points to an exceptional potential of TMDC excitons (stable electron-hole pairs)^[5] for ultra-efficient energy and information technologies,^[6,7] sensing,^[8] and fundamental studies of collective quantum phenomena.^[9,10] However, integration of monolayer TMDCs into useful electrical and optical devices by direct material deposition, for example, of high- κ dielectric materials for top-gating,^[11–13] usually degrades their

M. Wurdack, Dr. E. Estrecho, Dr. M. Pieczarka,^[†] Prof. E. A. Ostrovskaya
ARC Centre of Excellence in Future Low-Energy Electronics Technologies
and Nonlinear Physics Centre
Research School of Physics
The Australian National University
Canberra ACT 2601, Australia
E-mail: matthias.wurdack@anu.edu.au; elena.ostrovskaya@anu.edu.au
T. Yun

ARC Centre of Excellence in Future Low-Energy Electronics Technologies
and Department of Materials Science and Engineering
Monash University
Clayton, Australia

Dr. N. Syed, Dr. A. Zavabeti
Department of Chemical and Environmental Engineering
RMIT University
Melbourne VIC 3001, Australia

Dr. S. Bhattacharyya, Dr. S.-Y. Chen, Prof. M. S. Fuhrer
ARC Centre of Excellence in Future Low-Energy Electronics Technologies
and School of Physics and Astronomy
Monash University
Clayton VIC 3168, Australia

 The ORCID identification number(s) for the author(s) of this article can be found under <https://doi.org/10.1002/adma.202005732>.

^[†]Present address: Department of Experimental Physics, Wrocław University of Science and Technology, Wyb. Wyspiańskiego 27, Wrocław 50-370, Poland

DOI: 10.1002/adma.202005732

Dr. A. Zavabeti
Department of Chemical Engineering
The University of Melbourne
Parkville, VIC 3010, Australia

Dr. B. Haas, J. Müller
Institut für Physik & IRIS Adlershof
Humboldt-Universität zu Berlin
D-10099 Berlin, Germany

Dr. M. N. Lockrey
School of Mathematical and Physical Sciences
University of Technology Sydney
Ultimo, NSW 2007, Australia

Dr. Q. Bao
Department of Materials Science and Engineering
Monash University
Clayton, Australia

Prof. C. Schneider
Institut of Physics
Carl von Ossietzky University of Oldenburg
Ammerländer Heerstrasse 114-118, 26126 Oldenburg, Germany

Prof. C. Schneider
Technische Physik
Wilhelm-Conrad-Röntgen Research Center for Complex Material Systems
University of Würzburg
Am Hubland, D-97074 Würzburg, Germany

Dr. Y. Lu
ARC Centre of Excellence in Future Low-Energy Electronics Technologies
and Research School of Electrical, Energy and Materials Engineering
College of Engineering and Computer Science
The Australian National University
Canberra ACT 2601, Australia

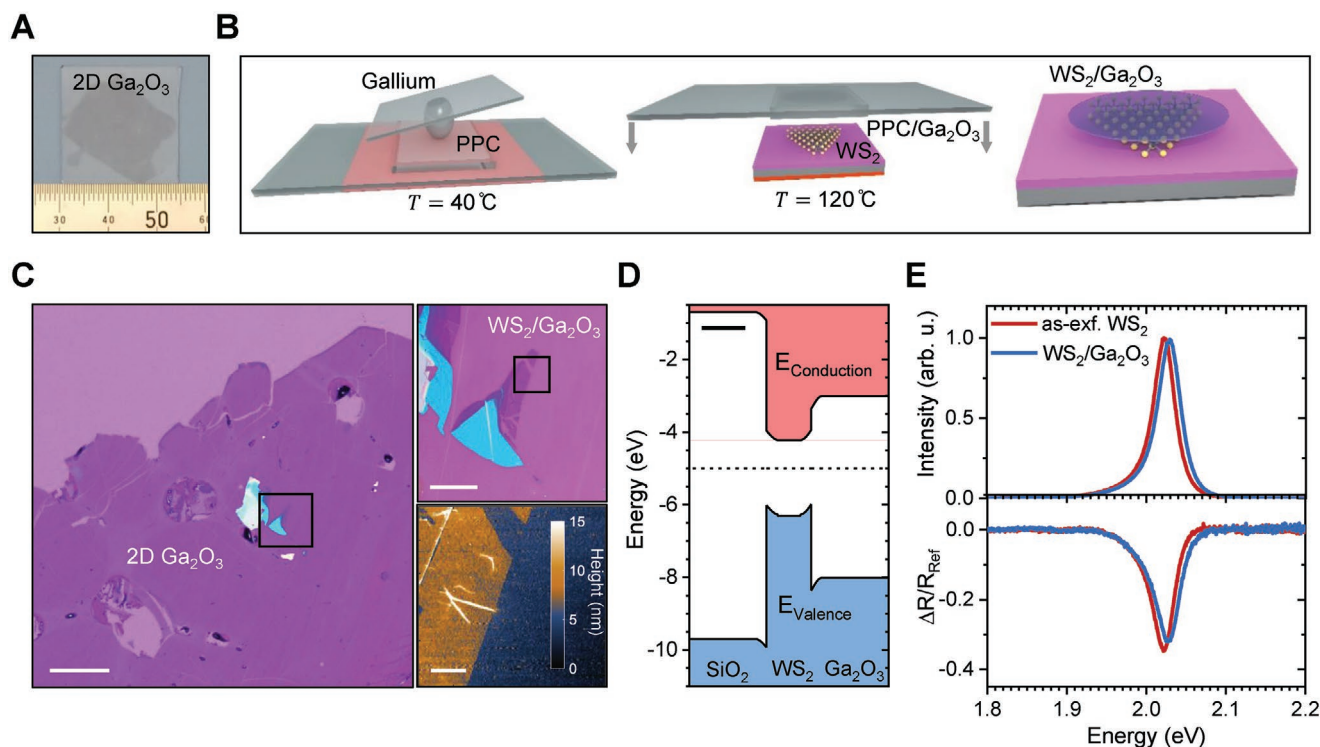


Figure 1. Large-scale passivation of monolayer WS₂ with ultrathin Ga₂O₃ glass. A) Camera image of a cm-sized Ga₂O₃ sheet on glass. The values on the ruler are in the mm scale. B) Schematics of the PPC-assisted deterministic transfer technique for TMDC/Ga₂O₃ heterostructures (from left to right). C) Microscopy and AFM images of a WS₂/Ga₂O₃ heterostructure (scale bar sizes: 200, 40, and 5 μm). D) Schematic band diagram of the WS₂/Ga₂O₃ heterostructure (scale bar size: 2 nm). E) PL and reflectivity spectra of an as-exfoliated monolayer WS₂ and of a WS₂/Ga₂O₃ heterostructure under ambient conditions.

electronic and optical properties. High optical and electronic performance can be achieved and retained^[14,15] by full encapsulation in mechanically exfoliated hexagonal boron nitride (hBN), commonly used to passivate and protect the monolayers. However, this approach is inherently non-scalable since mechanical exfoliation leads to irregular-shaped crystals with inconsistent thickness and size. Significant effort has been directed toward increasing the size of monolayer TMDCs from several μm to the cm-scale,^[16,17] and the capability to passivate and protect the monolayers on similar scales is equally important. Without a large scale passivation and protection technology, the realization of multilayer structures with integrated monolayer TMDCs remains challenging and non-scalable.

A practical passivation and protection material should: a) have a uniform, nm-scale thickness on wafer scale, b) have no negative effects on the optical and electrical properties of monolayer TMDCs, and c) protect against further material

deposition to enable the integration into multilayer heterostructures. While a large-scale passivation of MoSe₂ can be achieved by using the larger-bandgap TMDC MoS₂,^[18] large-scale passivation and protection with a wide-bandgap material potentially applicable for all TMDCs is not yet available. Here, we introduce an isotropic, ultrathin Ga₂O₃ glass^[19] as a novel material for low-cost passivation and protection of atomically thin semiconductors. Traditionally, research into 2D materials focuses on crystalline materials. Fully amorphous ultrathin materials that feature a glass-like structure are rarely investigated but possess intriguing and useful properties.^[20] The wide-bandgap ultrathin Ga₂O₃ glass can be synthesized under ambient conditions, with a highly reproducible nm-scale thickness on cm-scale. By capping the notoriously fragile WS₂ with Ga₂O₃, we demonstrate its excellent passivating properties. Our measurements at cryogenic temperatures indicate that the Ga₂O₃ passivates the commercial grade WS₂ monolayer by filling in sulphide vacancies. The passivated WS₂ exhibits enhanced exciton photoluminescence (PL) and suppressed exciton annihilation processes, similarly to the effects of superacid treatment^[21] and full hBN encapsulation.^[22] Finally, we show that Ga₂O₃ protects WS₂ against further deposition of Al₂O₃, a high-κ dielectric material. Comparison of the exciton PL of commercial grade monolayer WS₂ capped by either Ga₂O₃ or hBN shows that the Ga₂O₃ glass outperforms hBN as a protective material at room temperature.

Amorphous Ga₂O₃ is an electrically insulating, isotropic glass, fully transparent in the visible range,^[23] and is therefore well suited for protection of optically active materials. The recently discovered

Prof. A. G. Truscott
Laser Physics Centre
Research School of Physics
The Australian National University
Canberra ACT 2601, Australia
Dr. T. Daeneke
ARC Centre of Excellence in Future Low-Energy Electronics Technologies
and Department of Chemical and Environmental Engineering
RMIT University
Melbourne VIC 3001, Australia
E-mail: torben.daeneke@rmit.edu.au

liquid metal printing method^[19] enables the low-cost synthesis of cm-sized ultrathin sheets of Ga₂O₃ (Figure 1A). Atomic force microscopy (AFM) measurements performed on multiple Ga₂O₃ sheets confirm their uniform thickness ($t \approx 2.98 \pm 0.10$ nm), self-limited by the Cabrera–Mott mechanism^[19] (see S1, Supporting Information). X-ray photoelectron spectroscopy (XPS) on the Ga₂O₃ confirms the purity of its stoichiometric composition with 60% oxygen and 40% gallium (see S2, Supporting Information). A scanning electron microscope with a transmission diffraction stage was used to measure the crystal structure of synthesized Ga₂O₃, revealing that it is an entirely amorphous, isotropic glass (see S3, Supporting Information), stable in a wide temperature range (see S4, Supporting Information). Electron energy loss spectroscopy (EELS) measurements unveiled a bandgap of around 5.1 eV (see S5, Supporting Information).

We have developed two high-yield techniques for capping monolayer TMDCs with the Ga₂O₃ glass. The first technique is the direct synthesis of Ga₂O₃ on top of the monolayers, capable of covering large-area TMDCs, for example, grown by chemical vapor deposition (CVD) (see S6 and S7, Supporting Information). The second technique (Figure 1B) is the deterministic transfer of the Ga₂O₃, synthesized on spin-coated polypropylene carbonate (PPC), onto target areas, such as μm -sized mechanically exfoliated monolayers (S8, Supporting Information). These methods were used to create the WS₂/Ga₂O₃ heterostructures with both CVD-grown and exfoliated monolayers. Monolayer WS₂ features the largest band gap in the TMDC family,^[4] and therefore enables us to test whether Ga₂O₃ glass sufficiently confines the excited charge carriers in the TMDCs. In what follows, we focus on monolayer WS₂ mechanically exfoliated from single-crystalline commercial grade bulk crystals, which have superior optical quality compared to the large-scale CVD-grown monolayers used in this work.

Figure 1C shows a clean millimeter-scale sheet of Ga₂O₃ deterministically transferred on top of an exfoliated monolayer WS₂ (see S9, Supporting Information for the results on CVD-grown WS₂). The AFM image of the sample surface shows a homogeneous monolayer coverage. A careful analysis of the step-profile of a WS₂/Ga₂O₃ heterostructure can be found in S1, Supporting Information. The XPS and EELS measurements shown in S1 and S4, Supporting Information, together with the known material properties of monolayer WS₂,^[24,25] amorphous SiO₂,^[26] and amorphous Ga₂O₃,^[23] allow us to construct a band diagram of the WS₂/Ga₂O₃ heterostructure (see Figure 1D), while the exact position of the WS₂ band edge is still under debate.^[5,24,25] The identified type I band alignment enables the Ga₂O₃ to confine the free carriers in the conduction and valence bands of WS₂, to form excitons.

To test the effect of the Ga₂O₃ capping on the exciton properties of monolayer WS₂, we performed PL and reflectivity studies. The system was excited by a ND:YAG continuous wave (cw) laser source with a wavelength of $\lambda = 532$ nm ($E \approx 2.33$ eV) which is energetically above the band gap of monolayer WS₂, but below the band gap of the ultrathin Ga₂O₃. The reflectivity measurements were performed with a tungsten halogen white light source. The PL and reflectivity spectra of an as-exfoliated monolayer WS₂ and of the WS₂/Ga₂O₃ heterostructure under ambient conditions feature the exciton PL and absorption at $E \approx 2.01$ eV (Figure 1E). The excitons in WS₂/Ga₂O₃ have slightly higher energies compared to the as-exfoliated WS₂, most likely due to dielectric screening effects in Ga₂O₃. Nevertheless, the amplitude

and the linewidth of the PL and reflectivity spectra are not affected by Ga₂O₃ capping, indicating that the WS₂ excitons are not quenched. The PL and Raman measurements on the CVD-grown monolayers confirm these results, and show that the optical phonon modes of monolayer WS₂ remain intact (see S9, Supporting Information). By contrast, the exciton PL of exfoliated WS₂ monolayers passivated with the commercial grade hBN is significantly quenched (see S10, Supporting Information).

The effect of the Ga₂O₃ capping on the WS₂ exciton PL and absorption was further tested at $T = 4.3$ K, when exciton–phonon interactions and thermal effects are suppressed. We excited the as-exfoliated WS₂ and the heterostructure with a large Gaussian laser spot of the diameter ≈ 25 μm , which effectively eliminated artefacts due to the sample inhomogeneities by averaging the PL over a large sample area. Figure 2A contains the corresponding PL intensity maps, showing that both the as-exfoliated WS₂ and the heterostructure have a homogeneous PL texture. The PL spectra of the monolayers (Figure 2B) are composed of multiple distinct PL peaks, including the exciton ($E_X \approx 2.09$ eV), the trion ($E_T \approx 2.06$ eV), and additional low-energy peaks associated with many-body complexes.^[4,27,28] The reflectivity spectra (Figure 2C) of the exfoliated monolayers show strong absorption features at the exciton and trion energies, which indicates that both the uncapped and the capped samples are doped.^[14] Since the ratios between the absorption dips for both samples are the same, this effect is not related to the Ga₂O₃ capping and can be traced to the large density of sulphide vacancies in the commercial grade monolayer WS₂ resulting in high intrinsic n-type doping.^[29]

The PL intensity of the heterostructure is strongly enhanced at cryogenic temperatures (see Figure 2A,B and S9 and S11, Supporting Information). In particular, at low excitation intensities, the broad bound exciton peak, which dominates the PL spectrum of the as-exfoliated sample around 146 meV below the free exciton energy,^[30] is strongly quenched while the PL of the excitons, trions, and low-energy states are enhanced (Figure 2D). This indicates that Ga₂O₃ capping suppresses formation of bound excitons at sulphide vacancies,^[31] enhancing the formation of many-body states and the total exciton quantum yield. Indeed, cathodoluminescence (CL) measurements at $T = 70$ K presented in S12, Supporting Information, reveal the presence of deep donor-type oxide vacancies in Ga₂O₃,^[32] with a change of the density and distribution of the vacancies in the WS₂/Ga₂O₃ heterostructure. This result suggests that oxides in the Ga₂O₃ passivate sulphide vacancies in the WS₂, possibly through hydrogen-like bonds, changing the density and distribution of the oxygen vacancies in the Ga₂O₃ sheet. This mechanism can explain the suppression of bound exciton formation in the WS₂/Ga₂O₃, without affecting its doping level. The exact nature of the bonding between the WS₂ and the Ga₂O₃ is the subject of future work.

To understand the origins of the PL enhancement, we measured the exciton PL of both the as-exfoliated WS₂ and the WS₂/Ga₂O₃ heterostructure for a range of laser intensities I_L spanning two orders of magnitude (Figure 2E). Corresponding PL spectra are shown in S11, Supporting Information. At laser intensities below ≈ 10 $\mu\text{W } \mu\text{m}^{-2}$, the exciton intensity of the uncapped monolayers follows the power law, $I_X \propto I_L^2$, shown by the dashed lines in Figure 2E. Without losses, and assuming the direct photon–exciton transition, the dependence

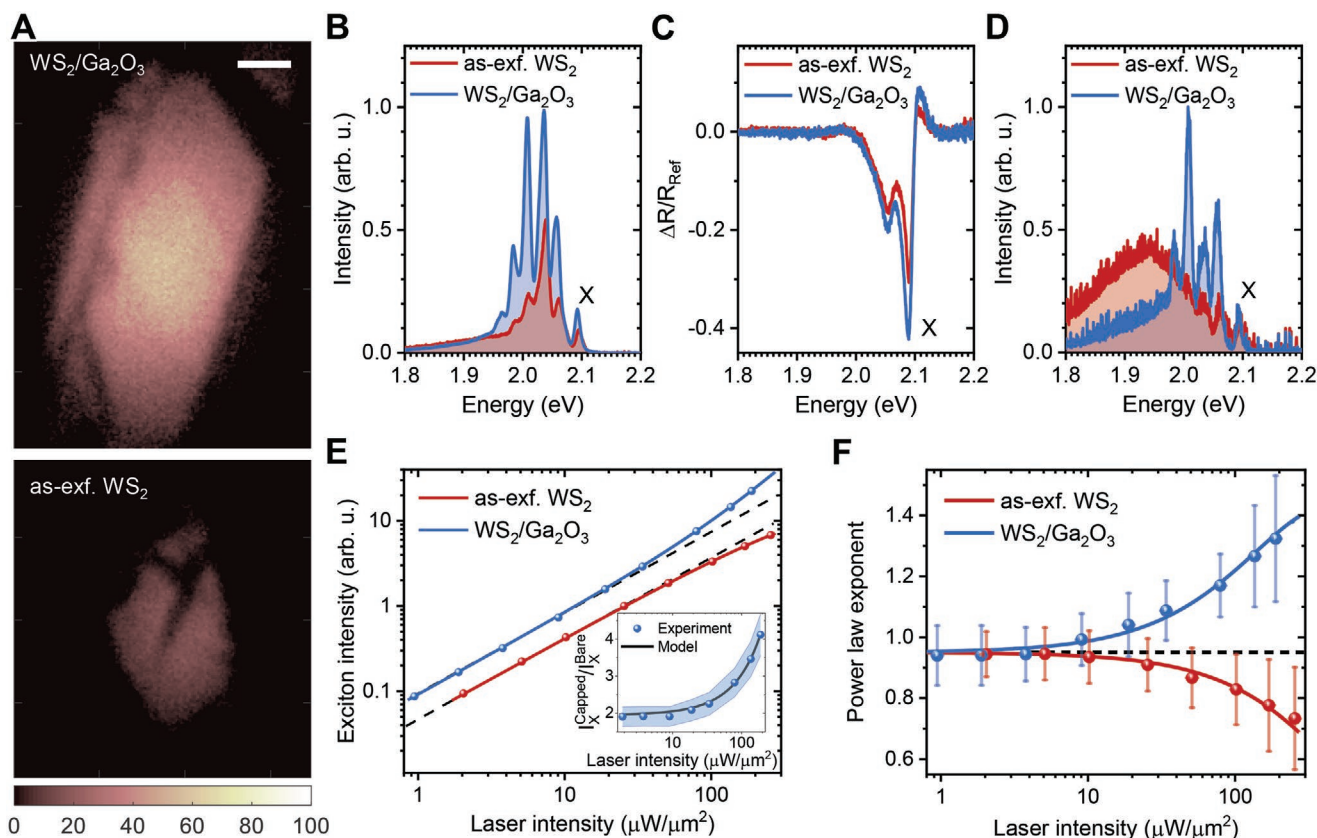


Figure 2. PL studies on a WS₂/Ga₂O₃ heterostructure at $T = 4.3$ K: A) PL images of a WS₂/Ga₂O₃ heterostructure and of an as-exfoliated monolayer WS₂ under large Gaussian laser spot excitation (≈ 25 μm), the scale bar size is 5 μm; B) corresponding PL spectra with $I_L \approx 34$ μW μm⁻²; C) laser intensity dependent exciton PL intensities (dots) fitted with the model from S12, Supporting Information (solid line); (inset) exciton PL intensity ratios in the bare and the capped monolayers; D) extracted power law-exponent k (slope) for the exciton PL intensities. The dashed lines correspond to a power law exponent of $k = 0.95$.

is linear: $k = 1$.^[33] In our samples, at low laser intensities, $k \approx 0.95$, which indicates that the exciton formation experiences intensity-dependent losses, for example, free-to-bound exciton transitions or formation of many-body exciton complexes (Figure 2D). However, at laser intensities above ≈ 10 μW μm⁻², the exponent of the power law $k \propto \log I_X / \log I_L$ decreases for the as-exfoliated WS₂ (see Figure 2F), in line with previous observations.^[22] This behavior is typically caused by annihilation processes between multiple excitons or between excitons and defects,^[34] for example, Auger recombination.^[35]

In contrast, for the heterostructure, the power law exponent remains well above $k \approx 0.95$. This indicates that the exciton annihilation in monolayer WS₂ is suppressed by Ga₂O₃ capping, similarly to the effect of full hBN encapsulation.^[22,35] However, the mere suppression of annihilation would result in a linear power law with a constant $k \approx 1$,^[22] while in WS₂/Ga₂O₃ the exciton PL transitions from a linear to a nonlinear behavior with increasing laser intensities (Figure 3F). This transition can be explained by a two-step exciton generation process via the deep oxide vacancies in the Ga₂O₃ (see S13, Supporting Information), in addition to the direct electron–hole excitation. The indirect process involves electron tunnelling between the donor-type oxide vacancies and the WS₂ valence band as an intermediate step in the WS₂ exciton formation. This results in accumulation of exciton densities and growing enhancement of the exciton PL intensity.

By fitting the exciton intensities and the extracted power law exponents of both as-exfoliated WS₂ and the heterostructure (see Figure S2E,F, Supporting Information) with the theoretical model (see S13, Supporting Information), we deduce that the exciton generation rate in the heterostructure is 1.9 ± 0.3 times higher, and that the exciton saturation density dictated by the annihilation processes is 28 ± 3 times higher compared to the as-exfoliated WS₂. These accumulating effects lead to the observed power-dependent enhancement of the exciton PL intensity in WS₂/Ga₂O₃, with an enhancement factor of 4.1 ± 0.6 within our power range (Figure 2E, inset). Measurements on CVD-grown monolayer WS₂ show the same PL intensity enhancement at cryogenic temperatures (S9, Supporting Information).

To test the protective capacity of the ultrathin Ga₂O₃ for device integration, we deposited Al₂O₃, a high- κ dielectric material, onto monolayer WS₂ capped by either Ga₂O₃ or exfoliated commercial grade hBN (Figure 3A). For deposition, we used electron beam evaporation (EBE) with a relatively high electron beam energy to stress-test the protection. As seen in Figure 3B, direct EBE deposition of Al₂O₃ on top of bare WS₂ strongly quenches the exciton PL.^[11] The PL spectra (Figure 3C) of the hBN and Ga₂O₃ capped WS₂ after EBE of Al₂O₃ show that both methods protect well against further material deposition, with approximately two orders of magnitude enhancement of exciton PL intensities compared to WS₂/Al₂O₃.

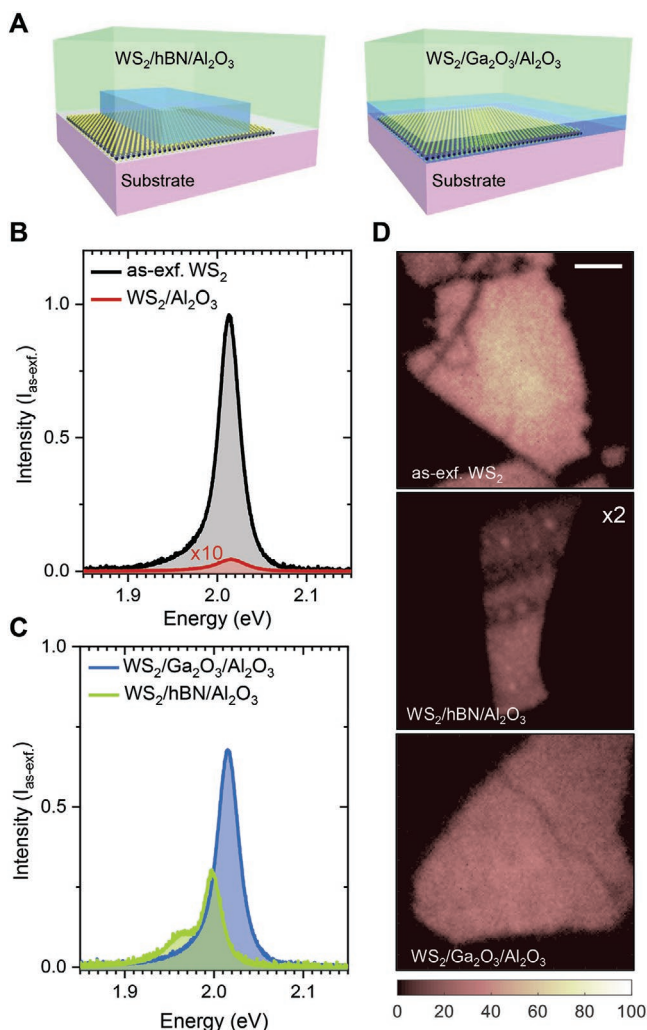


Figure 3. Integration of monolayer WS₂ in a high- κ dielectric environment: A) Schematics of WS₂/hBN/Al₂O₃ and WS₂/Ga₂O₃/Al₂O₃ heterostructures on SiO₂ substrates; B) PL spectra of monolayer WS₂ on SiO₂ before (as-exfoliated) and after Al₂O₃ deposition by EBE; C) PL spectra of WS₂/hBN/Al₂O₃ and WS₂/Ga₂O₃/Al₂O₃ heterostructures; D) PL intensity maps of as-exfoliated WS₂, and WS₂/hBN/Al₂O₃ and WS₂/Ga₂O₃/Al₂O₃ heterostructures under Gaussian spot excitation ($\approx 25 \mu\text{m}$). PL intensity of WS₂/hBN/Al₂O₃ is multiplied by a factor of 2. The scale bar size is $5 \mu\text{m}$.

However, the PL spectrum of the hBN-capped WS₂ (Figure 3C) shows a pronounced shoulder at the trion energy ($E_T \approx 1.96 \text{ eV}$), which indicates that it is strongly doped after Al₂O₃ deposition process, similarly to the effect observed in vacuum (see S9, Supporting Information). In addition, the hBN flake covers the monolayer only partially, resulting in a relatively small protected area (Figure 3D). In contrast, the PL spectrum of the WS₂/Ga₂O₃/Al₂O₃ heterostructure shows strong neutral exciton PL with around 70% of the exciton intensity of an as-exfoliated WS₂ monolayer. The PL texture of the WS₂/Ga₂O₃/Al₂O₃ is homogeneous (Figure 3D), which highlights the homogeneity of the coverage. The PL measurements on Ga₂O₃-capped CVD-grown monolayer WS₂ support these observations (see S9, Supporting Information).

To summarize, the novel ultrathin Ga₂O₃ glass shows great potential as a low-cost and practical wide-bandgap, isotropic material for scalable passivation of monolayer WS₂. Capping the monolayers with Ga₂O₃, either by direct printing or by deterministic transfer, fully preserves their exciton properties in ambient conditions. At cryogenic temperatures, the Ga₂O₃ passivation significantly enhances the optical performance of WS₂ by suppressing bound exciton formation at the sulphide vacancies, promoting nonlinear exciton generation, and suppressing the exciton annihilation processes. These findings provide a pathway toward high-performance surface-passivated TMDC/Ga₂O₃ heterostructures on a cm-scale, for example, by combining the large-scale mechanical exfoliation^[17] with the Ga₂O₃ capping. Finally, our finding that the Ga₂O₃ glass outperforms hBN for protecting commercial grade monolayer WS₂ against high- κ dielectric material deposition (e.g., for top-gating) breaks new ground for the transition from surface TMDC-based devices with small functional areas to large-area devices fully encapsulated in a dielectric environment.

Supporting Information

Supporting Information is available from the Wiley Online Library or from the author.

Acknowledgements

This work was supported by the Australian Research Council (ARC) through the Centre of Excellence grant CE170100039. T.D. acknowledges funds received for the ARC DECRA Project DE190100100. C.S. gratefully acknowledges funding by the European Research Council (Project unLiMIt-2D, Grant No: 679288). B.H and J.M. acknowledge funding in the framework of the German Science Foundation (DFG) project “BerlinEM Network” (grant number KO2911/13-1) and SFB951 HIOS (project number 182087777), respectively. M.N.L. acknowledges funding by the ARC project LE180100030. M.P. acknowledges support by the Foundation for Polish Science (FNP) in the START programme. The authors are grateful to Dr. Aaron Elbourne for providing support with atomic force microscope measurements, to A/Prof. Sumeet Walia and Dr. Daniel Gomez for providing access to experimental equipment, to Dr. Alexey Chernikov for fruitful discussions, and to Mr. Wendi Ma for providing support with sample fabrication. The authors appreciate the use of the Australian National Fabrication Facility (ANFF) at its nodes in the Australian Capital Territory, Victoria, and New South Wales at University of Technology Sydney.

Conflict of Interest

The authors declare no conflict of interest.

Keywords

atomically thin semiconductors, device integration, exciton enhancement, passivation, 2D materials, transition metal dichalcogenides

Received: August 24, 2020

Revised: October 31, 2020

Published online: December 4, 2020

- [1] K. F. Mak, J. Shan, *Nat. Photonics* **2016**, *10*, 216.
- [2] Q. H. Wang, K. Kalantar-Zadeh, A. Kis, J. N. Coleman, M. S. Strano, *Nat. Nanotechnol.* **2012**, *7*, 699.
- [3] A. K. Geim, I. V. Grigorieva, *Nature* **2013**, *499*, 419.
- [4] T. Mueller, E. Malic, *npj 2D Mater. Appl.* **2018**, *2*, 29.
- [5] A. Chernikov, T. C. Berkelbach, H. M. Hill, A. Rigosi, Y. Li, O. B. Aslan, D. R. Reichman, M. S. Hybertsen, T. F. Heinz, *Phys. Rev. Lett.* **2014**, *113*, 076802.
- [6] K. F. Mak, K. L. McGill, J. Park, P. L. McEuen, *Science* **2014**, *344*, 1489.
- [7] B. Radisavljevic, A. Radenovic, J. Brivio, V. Giacometti, A. Kis, *Nat. Nanotechnol.* **2011**, *6*, 147.
- [8] S. Manzeli, D. Dumcenco, G. Migliato Marega, A. Kis, *Nat. Commun.* **2019**, *10*, 4831.
- [9] Z. Wang, D. A. Rhodes, K. Watanabe, T. Taniguchi, J. C. Hone, J. Shan, K. F. Mak, *Nature* **2019**, *574*, 76.
- [10] M. M. Fogler, L. V. Butov, K. S. Novoselov, *Nat. Commun.* **2014**, *5*, 4555.
- [11] S. Y. Kim, H. I. Yang, W. Choi, *Appl. Phys. Lett.* **2018**, *113*, 133104.
- [12] K. M. Price, S. Najmaei, C. E. Ekuma, R. A. Burke, M. Dubey, A. D. Franklin, *ACS Appl. Nano Mater.* **2019**, *2*, 4085.
- [13] J.-G. Song, S. J. Kim, W. J. Woo, Y. Kim, I.-K. Oh, G. H. Ryu, Z. Lee, J. H. Lim, J. Park, H. Kim, *ACS Appl. Mater. Interfaces* **2016**, *8*, 28130.
- [14] M. Sidler, P. Back, O. Cotlet, A. Srivastava, T. Fink, M. Kroner, E. Demler, A. Imamoglu, *Nat. Phys.* **2017**, *13*, 255.
- [15] J. Gu, B. Chakraborty, M. Khatoniar, V. M. Menon, *Nat. Nanotechnol.* **2019**, *14*, 1024.
- [16] J. Lee, S. Pak, P. Giraud, Y.-W. Lee, Y. Cho, J. Hong, A.-R. Jang, H.-S. Chung, W.-K. Hong, H. Y. Jeong, H. S. Shin, L. G. Ochipinti, S. M. Morris, S. N. Cha, J. I. Sohn, J. M. Kim, *Adv. Mater.* **2017**, *29*, 1702206.
- [17] F. Liu, W. Wu, Y. Bai, S. H. Chae, Q. Li, J. Wang, J. Hone, X.-Y. Zhu, *Science* **2020**, *367*, 903.
- [18] A. Surrente, D. Dumcenco, Z. Yang, A. Kuc, Y. Jing, T. Heine, Y.-C. Kung, D. K. Maude, A. Kis, P. Plochocka, *Nano Lett.* **2017**, *17*, 4130.
- [19] A. Zavabeti, J. Z. Ou, B. J. Carey, N. Syed, R. Orell-Trigg, E. L. H. Mayes, C. Xu, O. Kavehei, A. P. O'Mullane, R. B. Kaner, K. Kalantar-zadeh, T. Daeneke, *Science* **2017**, *358*, 332.
- [20] C.-T. Toh, H. Zhang, J. Lin, A. S. Mayorov, Y.-P. Wang, C. M. Orofeo, D. B. Ferry, H. Andersen, N. Kakenov, Z. Guo, I. H. Abidi, H. Sims, K. Suenaga, S. T. Pantelides, B. Özyilmaz, *Nature* **2020**, *577*, 199.
- [21] M. Amani, D.-H. Lien, D. Kiriya, J. Xiao, A. Azcatl, J. Noh, S. R. Madhupathy, R. Addou, S. KC, M. Dubey, K. Cho, R. M. Wallace, S.-C. Lee, J.-H. He, J. W. Ager III, X. Zhang, E. Yablonovitch, A. Javey, *Science* **2015**, *350*, 1065.
- [22] Y. Hoshi, T. Kuroda, M. Okada, R. Moriya, S. Masubuchi, K. Watanabe, T. Taniguchi, R. Kitaura, T. Machida, *Phys. Rev. B* **2017**, *95*, 241403(R).
- [23] J. Kim, T. Sekiya, N. Miyokawa, N. Watanabe, K. Kimoto, K. Ide, Y. Toda, S. Ueda, N. Ohashi, H. Hiratsatsu, H. Hosono, T. Kamiya, *NPG Asia Mater.* **2017**, *9*, e359.
- [24] H. L. Zhuang, R. G. Hennig, *J. Phys. Chem. C* **2013**, *117*, 20440.
- [25] H. Terrones, F. López-Urías, M. Terrones, *Sci. Rep.* **2013**, *3*, 1549.
- [26] V. Astašauskas, A. Bellissimo, P. Kuksa, C. Tomastik, H. Kalbe, W. S. M. Werner, *J. Electron Spectrosc. Relat. Phenom.* **2020**, *241*, 146829.
- [27] P. Nagler, M. V. Ballottin, A. A. Mitioglu, M. V. Durnev, T. Taniguchi, K. Watanabe, A. Chernikov, C. Schüller, M. M. Glazov, P. C. M. Christianen, T. Korn, *Phys. Rev. Lett.* **2018**, *121*, 057402.
- [28] S.-Y. Chen, T. Goldstein, T. Taniguchi, K. Watanabe, J. Yan, *Nat. Commun.* **2018**, *9*, 3717.
- [29] S.-S. Chee, C. Oh, M. Son, G.-C. Son, H. Jang, T. J. Yoo, S. Lee, W. Lee, J. Y. Hwang, H. Choi, B. H. Lee, M.-H. Ham, *Nanoscale* **2017**, *9*, 9333.
- [30] C. Cong, J. Shang, Y. Wang, T. Yu, *Adv. Optical Mater.* **2018**, *6*, 1700767.
- [31] V. Carozo, Y. Wang, K. Fujisawa, B. R. Carvalho, A. McCreary, S. Feng, Z. Lin, C. Zhou, N. Perea-López, A. L. Elías, B. Kabijs, V. H. Crespi, M. Terrones, *Sci. Adv.* **2017**, *3*, e1602813.
- [32] J. B. Varley, J. R. Weber, A. Janotti, C. G. V. d. Walle, *Appl. Phys. Lett.* **2010**, *97*, 142106.
- [33] C. Spindler, T. Galvani, L. Wirtz, G. Rey, S. Siebentritt, *J. Appl. Phys.* **2019**, *126*, 175703.
- [34] G. Moody, J. Schaibley, X. Xu, *J. Opt. Soc. Am. B* **2016**, *33*, C39.
- [35] J. Zipfel, M. Kulig, R. Perea-Causín, S. Brem, J. D. Ziegler, R. Rosati, T. Taniguchi, K. Watanabe, M. M. Glazov, E. Malic, A. Chernikov, *Phys. Rev. B* **2020**, *101*, 115430.